Preprint submitted to at-Automatisierungstechnik 2018

...

Christopher Schindlbeck*, Christian Pape, and Eduard Reithmeier

Multi-DOF Compensation of Piezoelectric Actuators with Recursive Databases

Mehrdimensionale Kompensation piezoelektrischer Aktoren mittels rekursiver Datenbasen

DOI ...
Received ...; accepted ...

Abstract: Piezoelectric actuators are subject to nonlinear effects when voltage-driven in open-loop control. In particular, hysteresis and creep effects are dominating nonlinearities that significantly deteriorate performance in tracking control scenarios. In this paper, we present an online compensator suitable for piezoelectric actuators that is based on the modified Prandtl-Ishlinskii model and utilizes recursive databases for the compensation of nonlinearities. The compensator scheme is furthermore extended to systems with more than one degree of freedom (DOF) such as Cartesian manipulators by employing a decoupling control design to mitigate inherent cross-coupling disturbances. In order to validate our theoretical derivations, experiments are conducted with coupled trajectories on a commercial 3-DOF micro-positioning unit driven by piezoelectric actuators.

Keywords: Piezoelectric Actuators, Hysteresis, Compensation, Decoupling control

1 Introduction

Piezoelectric actuators are subject to dominant nonlinear effects such as hysteresis and creep when driven in open-loop control by a voltage source. While it is possible to eliminate these effects by black-box control methodologies such as conventional PID control [1], these approaches are not able to give insight into the underlying mathematical model. An ubiquitous amount of models has been proposed to model hysteresis/creep effects and investigated for their inversion usability in order to feed-forward compensate these effects [2]. However, most models are not able to compensate hysteresis, asymmetric hysteresis, and creep effects at the same time while retaining online compensation capabilities. The analytically invertible modified Prandtl-Ishlinskii (mPI) model is able to realize this [3, 4]. To make this approach further robust for non-periodic trajectories where the ratio between creep and hysteresis also alters during trajectory execution, the idea of recursive databases was introduced in [5]. While research on the compensation of piezoelectric nonlinearities has been ongoing for decades, treating piezoelectric-driven stages

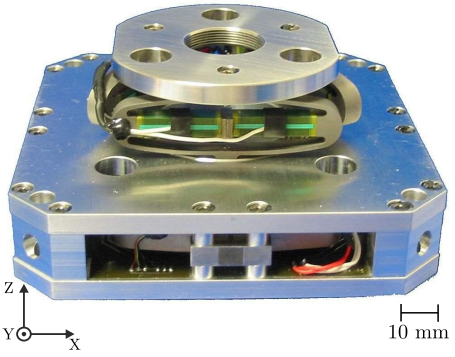

(a) Piezoelectric micro-positioning unit

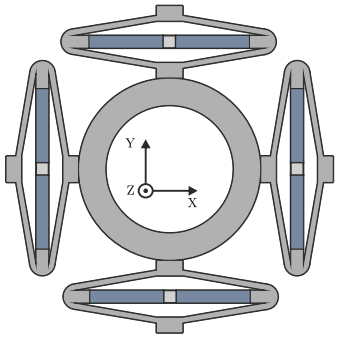

(b) Schematic cross-section of x-y-plane

Fig. 1: 3-DOF Piezoelectric micro-positioning unit (a) with schematic cross-section of the x-y-plane (b).

***Corresponding author: Christopher Schindlbeck,** Leibniz Universität Hannover, Institute of Measurement and Automatic Control, email: christopher.schindlbeck@imr.uni-hannover.de
Christian Pape, Eduard Reithmeier, Leibniz Universität Hannover, Institute of Measurement and Automatic Control

Preprint submitted to at-Automatisierungstechnik 2018

with multiple degrees of freedom (DOF) is a recent development. Therein, the goal is to mitigate cross-coupling effects that arise in these stages due to mechanical coupling between the axes. Fig. 1 shows such a multi-DOF piezoelectric-driven actuator. As the cross-section unveils, the end-effector is attached to multiple piezo-actuators which directly leads to cross-coupling effects (see Fig. 2). The cross-coupling compensation was treated for creep effects [6], for hysteresis effects with the help of the multivariate classical Prandtl-Ishlinskii model [7] and the Bouc-Wen model [8] as well as for compensation in flexure-based stages by superposition of backlash and deadzone operators [9]. In [10], a multivariate Hammerstein model was employed to treat the coupling problem.

Here, a compensation approach including decoupling based on the mPI model with recursive databases is presented. The key contributions of this paper are

- Online compensation of nonlinear piezoelectric effects including asymmetric hysteresis
- Compensation in tracking control scenarios with non-periodic trajectories based on recursive databases
- Robustness to changes in hysteresis/creep excitation
- Generalization to multi-DOF Cartesian manipulators by employing a decoupled control approach

Decoupling control strategies can be validated by using coupled trajectories such as rectangular trajectories [11] or Lissajous figures [7] and evaluating the normalized root-mean-square error (NRMSE) of the tracking error for quantification.

This paper is organized as follows. In Sec. 2, the mPI model is mathematically outlined. In Sec. 3, the desired compensator is derived by inverting the model. Furthermore, the decoupling approach is also presented therein. Experimental verification of the theoretical derivations is given in Sec. 4. Sec. 5 concludes the paper with a short summary and future work.

2 Modified Prandtl-Ishlinsikii Model

The mPI model is comprised of three different operators that account for the compensation of hysteresis, hysteretic asymmetry, and creep, respectively. In this paper, we will only treat the operators in their discrete form. A concise and brief review of the operators and the resulting mPI model is given within this section. For more details on the theoretical background and a thorough derivation, the interested reader is referred to [3, 5]. Throughout

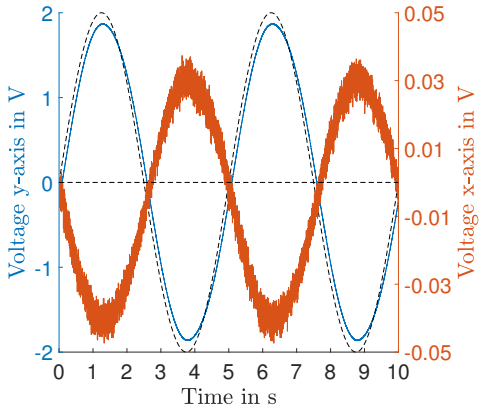

Fig. 2: Coupling problem: An excitation only on the y-axis (desired: black dotted, blue: actual) leads to undesired disturbance on x-axis (red).

the remainder of this paper, x denotes the input while y denotes the output of the operators. Conversely, y will be the compensator input and x its output.

2.1 mPI-Hysteresis Operator

The mPI-hysteresis operator $H_\delta[x(k), \mathbf{y}_{H0}]$ models symmetric hysteresis behavior. Therein, $\mathbf{y}_{H0}$ are the initial values. It consists of the weighted summation of elementary hysteresis operators

$$H_{r_H}[x(k), y(k-1)] = \max\{x(k) - r_H, \min\{x(k) + r_H, y(k-1)\}\}$$

each parameterized by a threshold r_H indicating its width (see Fig. 3a). The mPI-hysteresis operator can then be written in a compact form with weights $\mathbf{w}_H$ as

$$H_\delta[x(k), \mathbf{y}_{H0}] = \mathbf{w}_H^T \mathbf{H}_{\mathbf{r}_H}[x(k), \mathbf{y}_{H0}]. \tag{1}$$

2.2 mPI-Superposition Operator

Similarly, the mPI-superposition operator $S_\delta[x(k)]$ can be formed by a weighted summation as

$$S_\delta[x(k)] = \mathbf{w}_S^T \mathbf{S}_{\mathbf{r}_S}[x(k)] \tag{2}$$

with weights $\mathbf{w}_S$ and elementary superposition operators

$$S_{r_S}[x(k)] = \begin{cases} \max\{x(k) - r_S, 0\} & \text{for } r_S > 0 \\ \min\{x(k) - r_S, 0\} & \text{for } r_S < 0 \\ 0 & \text{for } r_S = 0. \end{cases}$$

Fig. 3b depicts this operator for three different parameterizations. The mPI-superposition operator is able to model

Preprint submitted to at-Automatisierungstechnik 2018

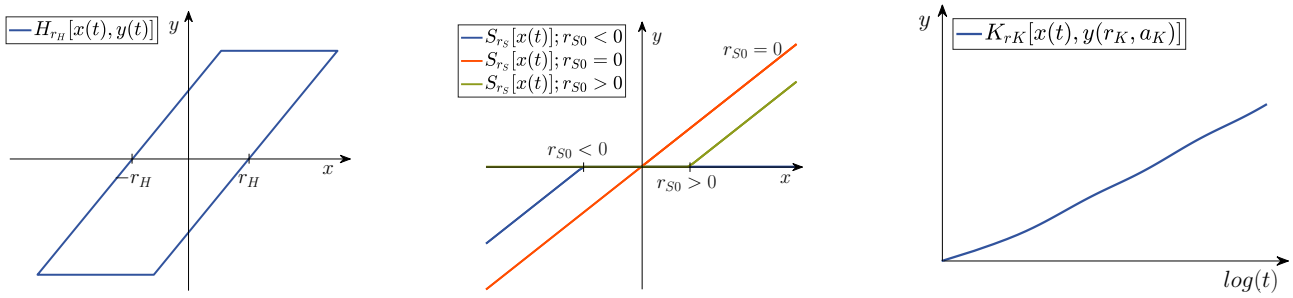

(a) mPI-Hysteresis Operator **(b)** mPI-Superposition Operator **(c)** mPI-Creep Operator

Fig. 3: Schematic illustration of elementary operators responsible for hysteresis (a), asymmetric hysteresis (b), and creep (c) modeling.

asymmetric hysteresis in combination with the aforementioned mPI-hysteresis operator.

2.3 mPI-Creep Operator

The mPI-creep operator is also computed by a weighted summation as

$$K_\delta[x(k), \mathbf{Y}_{K0}] = \mathbf{w}_K^T \mathbf{K}_{\mathbf{r}_K}[x(k), \mathbf{Y}_{K0}]. \tag{3}$$

with weights $\mathbf{w}_K$. Therein, the elementary creep operator $K_{r_K}[x(k), \mathbf{y}_{K0}(r_K)]$ is defined as

$$K_{r_K}[x(k), \mathbf{y}_{K0}(r_K)] = \frac{1}{m} \sum_{j=1}^{m} K_{r_K a_K}[x(k), y_{K0}(r_K, a_{Kj})]$$

where

$$K_{r_K a_K}[x(k), y(k), a_K] = y(k) + (1 - e^{-a_K T_s}) \cdot H_{r_K}[x(k) - y(k), 0],$$

is found by solving a differential equation where a_K are so-called creep eigenvalues. This operator, capable of modeling creep behavior over time, is shown in Fig. 3c.

2.4 Modified Prandtl-Ishlinskii Model

In order to obtain a unified piezoelectric model, the three aforementioned mPI operators can be combined as

$$\begin{aligned}\Gamma[x(k), \mathbf{y}_{H0}, \mathbf{Y}_{K0}] &= S_\delta[H_\delta[x(k), \mathbf{y_{H0}}] + K_\delta[x(k), \mathbf{Y}_{K0}]] \\ &= \mathbf{w}_S^T \mathbf{S}_{\mathbf{r}_S}(\mathbf{w}_H^T \mathbf{H}_{\mathbf{r}_H}[x(k), \mathbf{y}_{H0}] \\ &\quad + \mathbf{w}_K^T \mathbf{K}_{\mathbf{r}_K}[x(k), \mathbf{Y}_{K0}])\end{aligned} \tag{4}$$

yielding the final overall mPI model.

3 Online Compensation

In order to compensate the dominating nonlinear effects, the following measures are necessary. First, the inverse of the mPI model (4) needs to be established and secondly, the corresponding weights need to be identified during the trajectory execution. Afterwards, this single-axis compensation can be augmented with a decoupling design scheme to mitigate mechanical cross-coupling effects.

3.1 Inverse mPI Model

One of the advantages of the mPI model is that the inverse can be easily found in an algebraic manner without resorting to a cost-intensive numerical solution as compared to other approaches. The inverse of the mPI-hysteresis operator (1) is computed by

$$H_\delta^{-1}[y(k), \mathbf{z}'_{H0}] = \mathbf{w}'^T_H \mathbf{H}_{\mathbf{r}'_H}[y(k), \mathbf{z}'_{H0}] \tag{5}$$

with corresponding inverse weights $\mathbf{w}'_H$ and thresholds $\mathbf{r}'_H$. Similarly, the inverse of the mPI-superposition operator (2) is computed by

$$S_\delta^{-1}[y(k)] = \mathbf{w}'^T_S \mathbf{S}_{\mathbf{r}'_S}[y(k)] \tag{6}$$

with inverse weights $\mathbf{w}'_S$ and thresholds $\mathbf{r}'_S$. The inverse weights and thresholds can be found by an algebraic equation instead of computationally expensive numerical calculations [3]. With the help of (3), (6), and (5), the inverse of the mPI model (4) can be computed as

$$\begin{aligned}\Gamma^{-1}[y(k), \mathbf{y}'_{H0}, \mathbf{Y}'_{K0}] &= \\ &= H_\delta^{-1}\left[S_\delta^{-1}[y(k)] - K_\delta[x(k), \mathbf{Y}_{K0}], \mathbf{y}'_{H0}\right],\end{aligned} \tag{7}$$

which yields the compensator employed in Sec. 4 for compensation of piezoelectric nonlinearities.

3.2 Optimization with Recursive Databases

In order to obtain the weights, an optimization problem needs to be solved online[1]. The mPI model has the advan-

1 Online refers here to the calculation of the compensator during the operation of the piezoelectric actuator and not specifically to any real-time requirements.

Preprint submitted to at-Automatisierungstechnik 2018

tage that only a quadratic problem with linear inequality constraints needs to solved. The aforementioned operators and weights can be conveniently expressed as stacked vectors

$$\mathbf{\Phi}[x(k),y(k)] = \begin{pmatrix} \tilde{\mathbf{H}}_{\mathbf{r}_H}[x(k)] \\ -\mathbf{S}_{\mathbf{r}'_S}[y(k)] \\ \mathbf{K}_{\mathbf{r}_K}[x(k)] \end{pmatrix}, \ \mathbf{w} = \begin{pmatrix} \tilde{\mathbf{w}}_H \\ \mathbf{w}'_S \\ \mathbf{w}_K \end{pmatrix}$$

for the optimization procedure, where $\tilde{\mathbf{H}}_{\mathbf{r}_H}[x(k)]$ and $\tilde{\mathbf{w}}_H$ are the mPI-hysteresis operators and hysteresis weight vector each truncated by their first component. The cost function is a straightforward derivation from the requirement of minimizing the control error

$$E(k) = x(k) + \mathbf{w}^T \mathbf{\Phi}[x(k),y(k)]$$

and reads as

$$V = \frac{1}{2} \sum_{i=0}^{N_t-1} \sum_{k=iN_k}^{(i+1)N_k} E^2(k). \tag{8}$$

Therein, N_k denotes the discrete time interval of a database (in data points), and N_t the number of databases to be used in the compensation process [5]. The cost function (8) can be conveniently rearranged to a quadratic function by

$$V = \frac{1}{2}\mathbf{w}^T \underbrace{\sum_{i=0}^{N_t-1} \mathbf{A}_i}_{=:\mathbf{A}_{i+1}} \mathbf{w} + \underbrace{\sum_{i=0}^{N_t-1} \mathbf{b}_i^T}_{=:\mathbf{b}_{i+1}^T} \mathbf{w} + \frac{1}{2} \underbrace{\sum_{i=0}^{N_t-1} \mathbf{c}_i}_{=:\mathbf{c}_{i+1}}$$

with the definition of

$$\mathbf{A}_i = \sum_{k=iN_k}^{(i+1)N_k} \mathbf{\Phi}(k)\mathbf{\Phi}^T(k),$$

$$\mathbf{b}_i^T = \sum_{k=iN_k}^{(i+1)N_k} x(k)\mathbf{\Phi}^T(k), \text{ and } \mathbf{c}_i = \sum_{k=iN_k}^{(i+1)N_k} x^2(k)$$

in order to enable online computation capabilities. The weights obtained by this optimization procedure can then be inserted into the inverse model (7) to function as a feed-forward compensator[2].

3.3 Decoupled Control Design

The aforementioned compensation structure cancels out nonlinearities for each individual actuator. However, cross-coupling effects due to mechanical coupling of multi-DOF Cartesian manipulators are not addressed. For this, an appropriate decoupling strategy is necessary. Fig. 4 depicts the proposed decoupling scheme of this paper in combination with the mPI model for input-output linearization. Assuming that the transfer function of the piezoelectric actuators $\mathbf{G}(s)$ is sufficiently linearized by the presented compensation strategy (Sec. 3.2 and 3.1), the reference $\mathbf{R}(s)$ can be expressed by the input $\mathbf{Y}(s)$ by[3]

$$\mathbf{R}(s) = \begin{pmatrix} R_1(s) \\ R_2(s) \end{pmatrix} = \tag{9}$$
$$= \begin{bmatrix} G_{11}(s) & G_{12}(s) \\ G_{21}(s) & G_{22}(s) \end{bmatrix} \begin{pmatrix} Y_1(s) \\ Y_2(s) \end{pmatrix} = \mathbf{G}(s)\mathbf{Y}(s),$$

we can follow a linear diagonal decoupling approach with static-state feedback [12]. The goal is to find a feedback control matrix $\mathbf{C}(s)$ that maps the tracking error $\mathbf{E}(s)$ between reference and desired reference $\mathbf{R}_d(s)$ to compensator inputs by

$$\mathbf{Y}(s) = \mathbf{C}(s)\mathbf{E}(s) := \mathbf{C}(s)\left(\mathbf{R}_d(s) - \mathbf{R}(s)\right) \tag{10}$$

and diagonalizes the transfer function. This can be achieved via

$$\mathbf{C}(s) = \mathbf{G}^{-1}(s)\mathbf{G}_d(s),$$

where $\mathbf{G}_d(s) = \mathrm{diag}\{G_{11}(s), G_{22}(s)\}$ is the desired diagonalized transfer function matrix. In practical applications, cross-coupling effects exhibit a low signal-to-noise ratio (SNR) and therefore the measured output of the piezoelectric actuators needs to be filtered for feedback. This leads to the tracking error

$$\mathbf{E}(s) = \mathbf{R}_d(s) - \mathbf{G}_f(s)\mathbf{R}(s) \tag{11}$$

with filter transfer function $\mathbf{G}_f(s) = \mathrm{diag}\{G_f(s), G_f(s)\}$. Insertion of (11) into (10) and afterwards (10) into (9) yields the reference transfer function

$$\mathbf{G}_r(s) = \mathbf{G}_d(s)\left(\mathbf{I} + \mathbf{G}_d(s)\mathbf{G}_f(s)\right)^{-1}$$

which attenuates the reference signal by $\mathbf{R}(s) = \mathbf{G}_r(s)\mathbf{R}_d(s)$. In order to compensate this, an amplification transfer function $\mathbf{G}_a(s) = \mathbf{G}_r^{-1}(s)$ precedes the decoupling controller.

4 Experimental Results

In order to verify the compensator and the decoupling control strategy of Sec. 3, experimental results on a commercial micro-positioning unit are provided in this section.

2 Additionally, the weights are subject to constraints, which is out of the scope of this paper and the interested reader is referred to [3].

3 Here, the 2-DOF case will be treated due to the experimental validation in two dimensions. The extension to multiple DOF is straightforward.

Preprint submitted to at-Automatisierungstechnik 2018

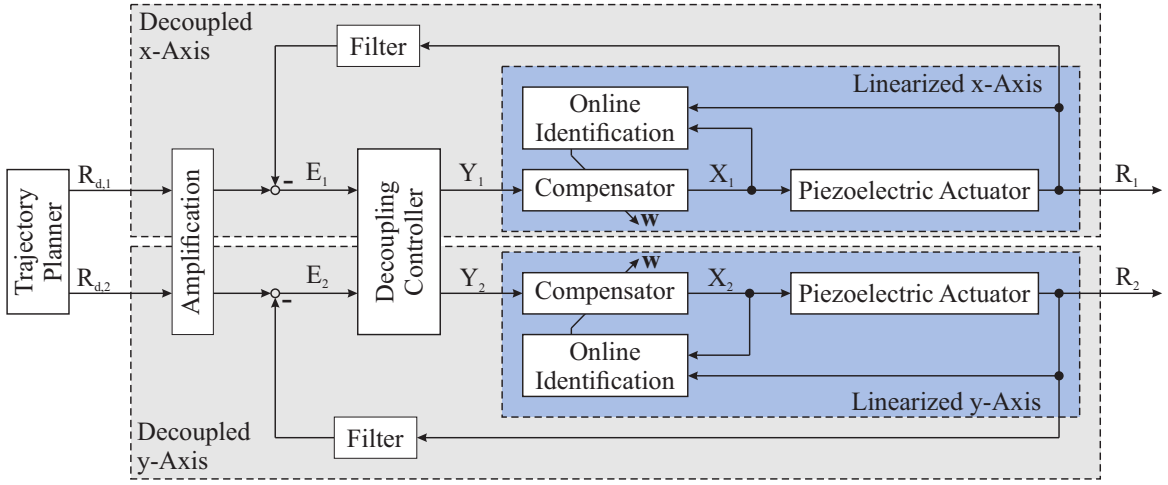

Fig. 4: Decoupling and compensation scheme for multi-DOF piezoelectric actuators (here exemplified for the 2-DOF case).

4.1 Setup

For experimental validation, we utilize the micro-positioning unit XYZ200M by *Cedrat Technologies* (see Fig. 1a). It is driven by piezoelectric actuators where each actuator is preloaded by an external elliptical spring shell made of stainless steel. This not only amplifies the displacement of the piezoelectric actuators by a factor of five but also protects e.g. against tensile stress. The x- and y-axes follow an antagonistic design (see Fig. 1b), i.e. two opposing piezoelectric actuators are employed for each axis, respectively. This enhances point-symmetry of the hysteresis curve but also induces disturbances due to mechanical cross-coupling, which will be treated by the aforementioned decoupling strategy. The micro-positioning unit has a nominal displacement of 200 µm and a nanoscopic resolution of 2 nm. Voltage input and strain-gauge measurements are commanded and accessed via a National Instruments real-time system, respectively.

4.2 Identification & Filtering

Identification is done in the frequency domain via a sinusoidal sweep and the transfer functions $G_{11}, G_{12}, G_{21}, G_{22}$ show almost linear behavior, see Fig. 5. For the control decoupling approach, each transfer function is approximated by a first-order all-pass filter. The fitting error in higher frequencies is caused by the first-order filter design and because more data points are recorded in the low-frequency domain. For pick-and-place applications, we are only interested in trajectories in the frequency range 0 Hz to 10 Hz.

As mentioned before, cross-coupling effects in piezoelectric actuators are characterized by a very low SNR. Therefore, appropriate filter design is crucial in order to yield satisfying decoupling behavior. In general, a trade-off has to be made between filter order, phase-lag, and real-time capabilities. Here we choose a low-order Bessel filter that on the one hand induces a low phase-lag and on the other hand its low order avoids real-time violations during the online filtering process.

Fig. 6 shows the efficacy of using the compensation in combination with decoupling approach. A sinusoidal wave is applied on the y-axis while the x-axis should show no signs of excitation. Without control approach and by only using the compensator, an undesired (albeit small) sine wave with 180° phase shift can be seen on the x-axis. Adding the decoupling strategy to the compensator significantly suppresses this undesired disturbance (SNR $\approx$ 1.36).

4.3 Coupled Trajectories

For further validation, four coupled trajectories are evaluated in this section:

1. Circle (x and y at 0.3 Hz, ±2 V)
2. Rectangle (x at ±1 V & y at ±2 V, both at 0.25 Hz)
3. Lissajous figure 1 (x at 0.2 Hz, ±2 V & y at 0.6 Hz, ±2 V)
4. Lissajous figure 2 (x at 0.5 Hz, ±1 V & y at 0.25 Hz, ±1 V)

Fig. 7 shows the results in the x-y-plane for these trajectories as well as close-up views at critical regions. Furthermore, the tracking error over time is depicted for better

Preprint submitted to at-Automatisierungstechnik 2018

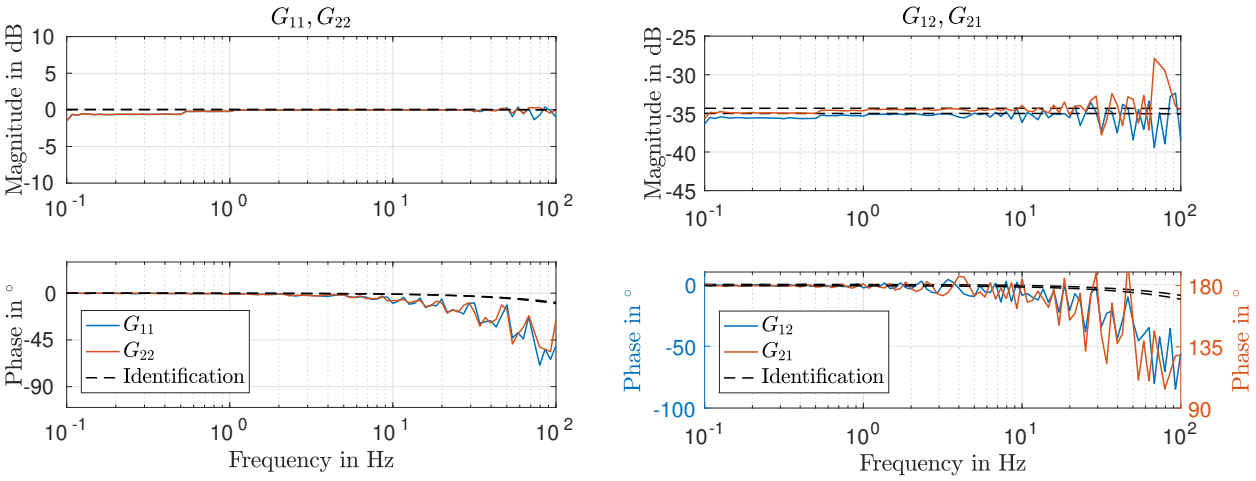

Fig. 5: Bode plots of diagonal transfer functions G_{11}, G_{22} (a) and off-diagonal transfer functions G_{12}, G_{21} (b).

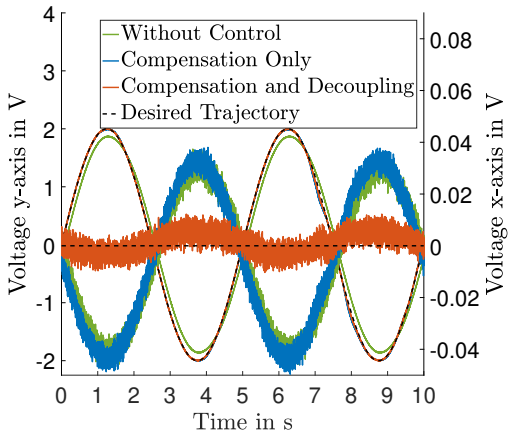

Fig. 6: Resolved coupling problem (see Fig. 2): Excitation on one axis leads to less undesired disturbance on other axis by employing the presented compensation and decoupling scheme.

Table 1: NRMSE of x- and y-axis for utilized trajectories without compensation (NRMSE), compensation without decoupling strategy (NRMSE_c), compensation including decoupling (NRMSE_{cd}), and percentual improvement ($\text{Impr.}_{c\to cd}$).

	NRMSE	NRMSE_c	NRMSE_{cd}	$\text{Impr.}_{c\to cd}$
***x*-Axis**				
Sinusoid	0.1299	0.0263	0.0163	37.88 %
Circle	0.1597	0.0251	0.0171	31.74 %
Rectangle	0.1256	0.0154	0.0112	27.30 %
Lissajous 1	0.1356	0.0224	0.0131	41.39 %
Lissajous 2	0.2082	0.0310	0.0116	62.50 %
***y*-Axis**				
Sinusoid	0.1201	0.0331	0.0198	40.01 %
Circle	0.1495	0.0283	0.0146	48.40 %
Rectangle	0.1961	0.0170	0.0165	2.94 %
Lissajous 1	0.1389	0.0322	0.0145	55.11 %
Lissajous 2	0.1851	0.0243	0.0095	60.83 %

comparability. For quantification of experimental results, the normalized root mean square error

$$\text{NRMSE}(y_d, y) = \|y_d - y\|_2 / \|y_d\|_2$$

can be evaluated. Based on this metric, Tab. 1 summarizes the experimental results which show that significant improvements of the tracking error for every trajectory have been made by adding the decoupling strategy to the compensation. The highest tracking error reduction can be observed for trajectories where there is a strong, permanent, and irregular coupling between the axes (such as the Lissajous figures). Trajectories where large portions are uncoupled (such as the rectangular trajectory) show less improvement.

5 Conclusion

In this paper, a model-based approach has been followed for the online compensation of piezoelectric nonlinearities. By augmenting it with a decoupling controller, mitigation of mechanical cross-coupling effects could be achieved. The subsequent experimental validation was executed on a commercial micro-positioning unit. By evaluating the NRMSE on four different coupled trajectories, significant improvements of the tracking error could be shown. Although the linear decoupling approach yielded good compensation results, a nonlinear decoupling approach might improve the mitigation of cross-coupling effects. Additionally, further improvement is potentially possible by using a high-order and adaptive filter.

Preprint submitted to at-Automatisierungstechnik 2018

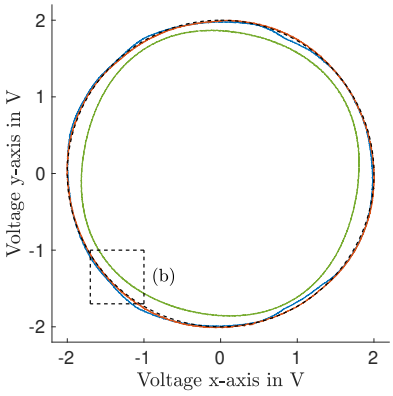

(a) Circle trajectory

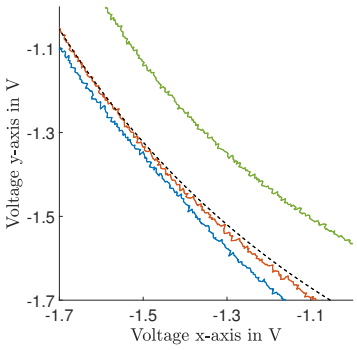

(b) Close-up of circle trajectory

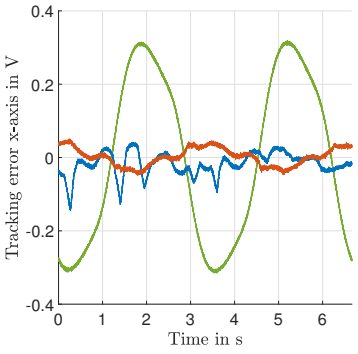

(c) Tracking error of circle trajectory

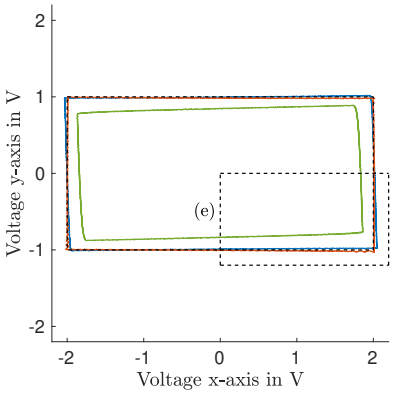

(d) Rectangle trajectory

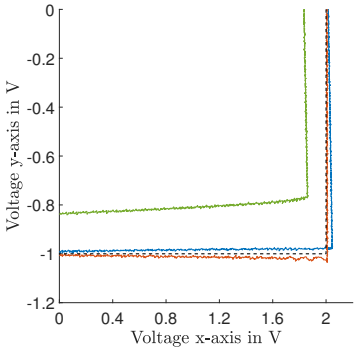

(e) Close-up of rectangle trajectory

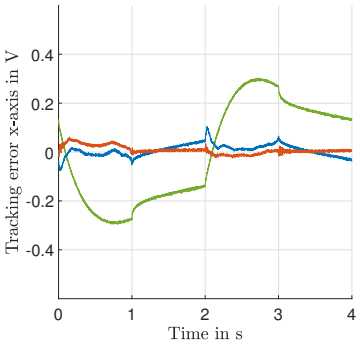

(f) Tracking error of rectangle trajectory

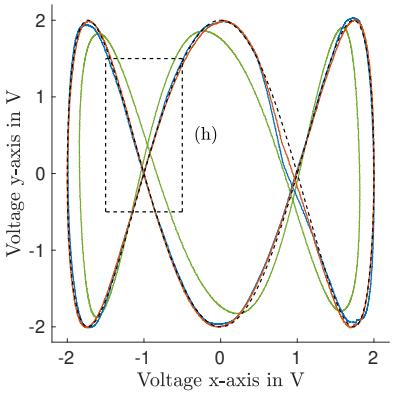

(g) Lissajous figure 1

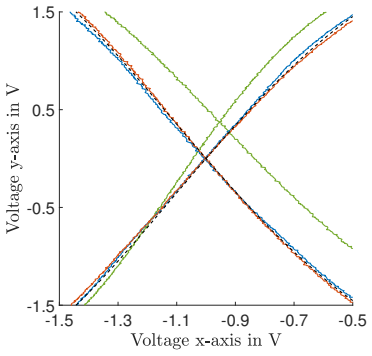

(h) Close-up of Lissajous figure 1

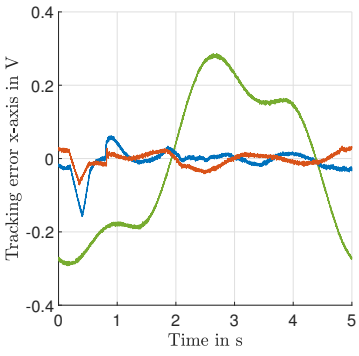

(i) Tracking error of Lissajous figure 1

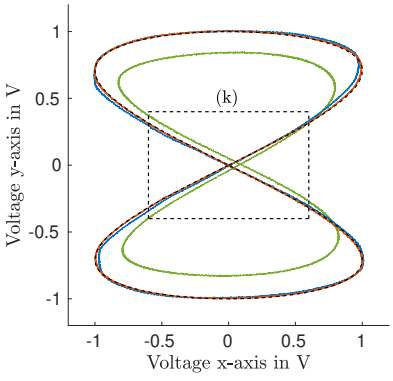

(j) Lissajous figure 2

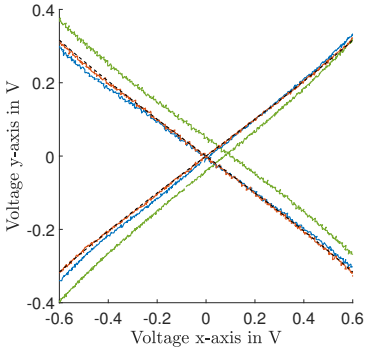

(k) Close-up of Lissajous figure 2

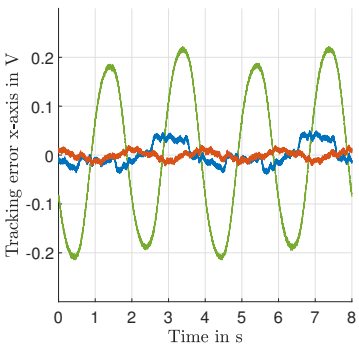

(l) Tracking error of Lissajous figure 2

Fig. 7: Four different trajectories (circle, rectangle, two Lissajous figures, see left column) with close-up views at critical regions (middle column), and tracking error (right column). Neither control nor compensation is shown in green, compensation only in blue, compensation with decoupling in red, and the desired trajectory by a dotted black line.

Preprint submitted to at-Automatisierungstechnik 2018

References

[1] C. Schindlbeck, A. Janz, C. Pape, and E. Reithmeier, "Increasing milling precision for macro-micro-manipulators with disturbance rejection control via visual feedback," in *IEEE/RSJ IROS*, 2017.

[2] G.-Y. Gu, L.-M. Zhu, C.-Y. Su, H. Ding, and S. Fatikow, "Modeling and control of piezo-actuated nanopositioning stages: A survey," *IEEE Trans. Automat. Sci. Eng.*, vol. 13, no. 1, pp. 313–332, 2016.

[3] K. Kuhnen, *Kompensation komplexer gedächtnisbehafteter Nichtlinearitäten in Systemen mit aktiven Materialien: Grundlagen - erweiterte Methoden - Anwendungen*, ser. Berichte aus der Steuerungs- und Regelungstechnik. Shaker, 2008.

[4] D. Pesotski, *Echtzeit-Kompensation von komplexen hysterese-und kriechbehafteten Nichtlinearitäten am Beispiel von Festkörperaktoren.* Logos Verlag Berlin GmbH, 2011.

[5] C. Schindlbeck, C. Pape, and E. Reithmeier, "Recursive online compensation of piezoelectric nonlinearities via a modified prandtl-ishlinskii approach," in *Proc. of the 20th IFAC World Congress, Toulouse*, 2017.

[6] M. Rakotondrabe, "Modeling and compensation of multivariable creep in multi-dof piezoelectric actuators," in *IEEE International Conference on Robotics and Automation*, 2012, pp. 4577–4581.

[7] ——, "Multivariable classical prandtl–ishlinskii hysteresis modeling and compensation and sensorless control of a nonlinear 2-dof piezoactuator," *Nonlinear Dynamics*, pp. 1–19, 2017.

[8] D. Habineza, M. Rakotondrabe, and Y. Le Gorrec, "Bouc–wen modeling and feedforward control of multivariable hysteresis in piezoelectric systems: application to a 3-dof piezotube scanner," *IEEE Transactions on Control Systems Technology*, vol. 23, no. 5, pp. 1797–1806, 2015.

[9] Z. Guo, Y. Tian, X. Liu, B. Shirinzadeh, F. Wang, and D. Zhang, "An inverse prandtl–ishlinskii model based decoupling control methodology for a 3-dof flexure-based mechanism," *Sensors and Actuators A: Physical*, vol. 230, pp. 52–62, 2015.

[10] B. Hu, H.-T. Zhang, and Z.-Y. Chen, "Nonlinear cross-coupling of a 2-dof piezoelectric actuator with multi-channel hammerstein model," in *IEEE Chinese Control Conference*, 2017, pp. 1196–1201.

[11] C. Schindlbeck, C. Pape, and E. Reithmeier, "Two degree-of-freedom online compensation of a piezoelectric micro-positioning unit," in *Proc. Appl. Math. Mech*, 2017.

[12] V. Kucera, "Diagonal decoupling of linear systems by static state feedback," *IEEE Transactions on Automatic Control*, 2017.

Dipl.-Tech. Math. Christopher Schindlbeck
Institute of Measurement and Automatic Control
Leibniz Universität Hannover
Nienburgerstr. 17
30167 Hannover
schindlbeck@imr.uni-hannover.de

Christopher Schindlbeck is a research assistant of the control engineering working group at the Institute of Measurement and Automatic Control at the Leibniz Universiät Hannover. He received his Diplom degree in mathematics in science and engineering at the Technical University of Munich in 2012. His research interests include control theory, robotics, optics, and machine learning.

Dr.-Ing. Christian Pape
Institute of Measurement and Automatic Control
Leibniz Universität Hannover
Nienburgerstr. 17
30167 Hannover
pape@imr.uni-hannover.de

Christian Pape is the head of the control engineering working group at the Institute of Measurement and Automatic Control at the Leibniz Universiät Hannover, where he worked in the robotics and control engineering lab and received his doctoral degree in 2011. His research interests include robotics and control engineering, image-based control and in-process metrology.

Prof. Dr.-Ing. Eduard Reithmeier
Institute of Measurement and Automatic Control
Leibniz Universität Hannover
Nienburgerstr. 17
30167 Hannover
reithmeier@imr.uni-hannover.de

Eduard Reithmeier has been the head of the Institute of Measurement and Automatic Control since 1996. Prior to this time, he was employed as the technical director of the Bodenseewerk Gerätetechnik GmbH. His current research interests include production metrology, in-process metrology, optical metrology, control engineering, active noise cancellation and biomedical engineering.